Morphological effect on the Raman frequency shift induced by tensile stress applied to crystalline polyoxymethylene and polyethylene: spectroscopic support for the idea of an inhomogeneous stress distribution in polymer material

Kohji Tashiro*, Gang Wu and Masamichi Kobayashi
Department of Macromolecular Science, Faculty of Science, Osaka University, Toyonaka, Osaka 560, Japan
(Received 11 January 1988; revised 16 February 1988; accepted 22 February 1988)

A tensile-stress-induced low-frequency shift was measured for the Raman bands of crystalline polyoxymethylene (POM) and polyethylene (PE) with different draw ratios λ. The apparent frequency-shift factor p $(=\Delta\tilde{\nu}/\Delta\sigma_{bulk})$ for the 539 cm^{-1} skeletal bending mode δ (COC) was found to become larger for the POM sample with lower λ: $p=-24\,cm^{-1}$/GPa ($\lambda=7$), -19 ($\lambda=17$) and -11 ($\lambda=34$). Such a difference in p was too small to detect for the skeletal stretching modes of PE samples with $\lambda=7$ to 100: $p=-6.0\,cm^{-1}$/GPa for ν_{as} (CC) at 1064 cm^{-1} and -4.5 for ν_s (CC) at 1131 cm^{-1}. This experimental fact, i.e. the dependence of the frequency-shift factor p on sample morphology, cannot be reasonably explained in terms of a homogeneous stress distribution or the simple mechanical series model of crystalline and amorphous phases. Based on the complex mechanical model (i.e. the parallel–series and series–parallel models), the Raman shift could be understood quantitatively, and the intrinsic shift factor α of the crystalline region was estimated as $-11\,cm^{-1}$/GPa for the δ (COC) mode of POM and as $-5.0\,cm^{-1}$/GPa for ν_{as} (CC) and $-3.8\,cm^{-1}$/GPa for ν_s (CC) of PE. A change in the Raman band profile under tensile stress was simulated and compared with the observed data.

(Keywords: polyoxymethylene; polyethylene; Raman spectra; tensile stress; morphology; mechanical model)

INTRODUCTION

In estimating a limiting Young's modulus of a polymer chain, an X-ray diffraction method under tensile stress has been playing an important role[1]. In this method the crystalline deformation is measured as a change in the Bragg angle, and Young's modulus is evaluated by dividing the stress σ_c by the strain ε_c, where σ_c and ε_c are the stress and strain, respectively, of the 'crystalline' phase. In this process we always encounter one serious problem: the assumption of a homogeneous stress distribution within the sample or the reasonableness of the so-called mechanical series model. In this model σ_c is equated with the stress σ_{bulk} applied to the bulk sample. Ward *et al.*[2] called the modulus thus obtained the apparent crystallite modulus E_c^{app} $(=\sigma_{bulk}/\varepsilon_c)$. The true crystallite modulus is defined as $E_c^{true}=\sigma_c/\varepsilon_c$. By measuring the X-ray diffraction of polyoxymethylene[2] and polyethylene[3] samples under tension, they found that E_c^{app} is dependent on the sample preparation conditions, such as draw ratio, and that E_c^{app} exhibits a remarkable temperature dependence in the vicinity of the glass transition temperature. They supported the so-called Takayanagi model in interpreting such behaviour of E_c^{app}. In recent X-ray measurements, Nakamae *et al.*[4,5] reported that ultra-drawn polyethylene and polyoxymethylene samples exhibit crystallite modulus values different from those of ordinarily prepared samples. Contrary to Ward *et al.*, they insisted on the reasonableness of the series model and ascribed such a difference in crystallite modulus to a difference in molecular motion in the crystalline region between ordinary and highly oriented samples. But they do not yet answer the naturally occurring question of why molecular motion of the polymer chain in the crystalline region must change from sample to sample. Thus there still remains the serious and unresolved problem of which mechanical model is more reasonable for interpreting the above-mentioned phenomena of the crystallite modulus.

In a series of papers[6–9] we have described the vibrational spectroscopic change induced by a tensile stress applied to oriented samples of polydiacetylene single crystal, ultra-drawn polyoxymethylene and ultra-drawn polyethylene. The infra-red and Raman bands of the skeletal vibrational modes were found to shift to the lower-frequency side with increasing tensile stress. These spectral changes are quite consistent with the lattice dynamical prediction for the deformation process of a stressed polymer chain[10]. In such a discussion, however, the frequency shift has been plotted against the bulk stress, not against the true crystalline stress, this being actually equivalent to a tacit utilization of the mechanical series model. In the measurement of the Raman spectra of stressed polyoxymethylene and polyethylene samples with different draw ratios, we have found that the frequency shift varies among the various samples. Since a

* To whom correspondence should be addressed

0032-3861/88/101768-11$03.00

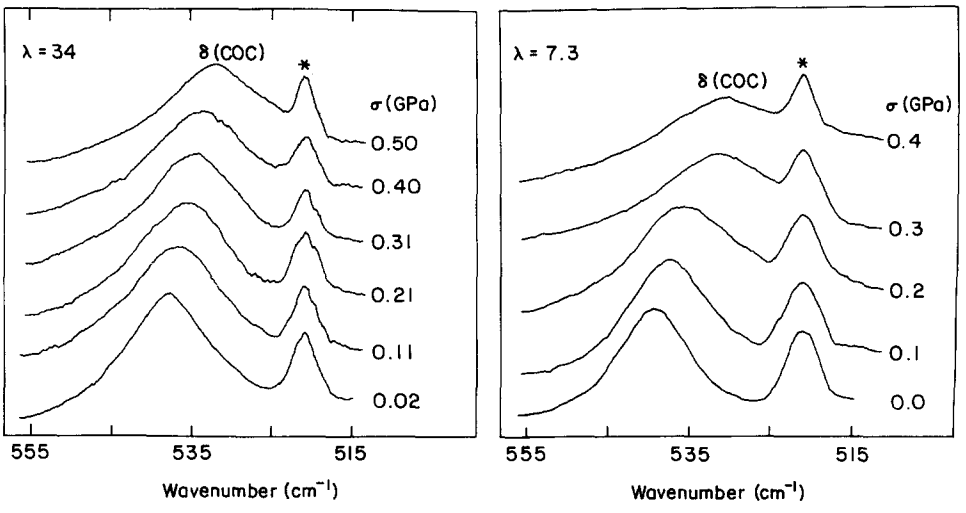

Figure 1 Polarized Raman spectra measured under tensile stress for POM samples with draw ratios of 7.3 and 34. An asterisk indicates the position of natural emission from Ar-ion laser

homogeneous stress distribution should result in the same frequency shift irrespective of sample morphology, these data require us to reinvestigate the assumption of the mechanical series model from the spectroscopic point of view, as described in the present paper.

EXPERIMENTAL

Samples

The polymers utilized in the present study were polyoxymethylene (POM) and polyethylene (PE).

POM. Three types of samples were employed: (a) Delrin rods with draw ratio $\lambda = 7.3$, prepared by stretching the melt-quenched sample at 160°C; (b) transparent rods (Tenac 3010, Asahi Chemical Co.) prepared by a 'pressurized drawing method' with $\lambda = 17$[11]; (c) rod samples (Tenac 5010) with $\lambda = 34$, prepared by drawing under the 'dielectric heating process' developed by NTT Co. Japan[12].

PE. Two samples have been used: (a) an ultra-drawn fibre from a dry gel, with $\lambda = 100$; (b) ordinarily stretched samples with $\lambda = 26$, 10 and 6.8. These latter samples were annealed at 85°C ($\lambda = 6.8$) or 120°C ($\lambda = 10$ and 26).

Measurements

Raman spectral measurements under tensile stress were performed using a stretching device reported in previous papers[6–9]. The 514.5 nm light from an argon-ion laser was utilized as an excitation beam and the spectra were recorded with Japan Spectroscopic Co. R500 and R1000 Raman spectrophotometers. Since the frequency shift induced by the tensile stress is not very large, the external signal of the natural laser emission was used as the frequency standard.

RESULTS AND DISCUSSION

Raman band shift induced by tensile stress

POM. In *Figure 1* are shown the Raman spectral changes of the oriented POM samples measured for the skeletal deformation band δ (COC) at 539 cm^{-1}. The band indicated by an asterisk is from the natural emission of the laser. As the tensile stress is increased, the band peak position shifts towards the lower-frequency side. At the same time the band profile gradually becomes broader, although the absolute intensity change cannot be compared among the different stressed states because the optical conditions might not necessarily be constant throughout the measurements. In *Figure 2* is plotted the peak frequency against the applied bulk stress σ for the three kinds of POM samples. The initial slope or the frequency-shift factor is found to be different for the

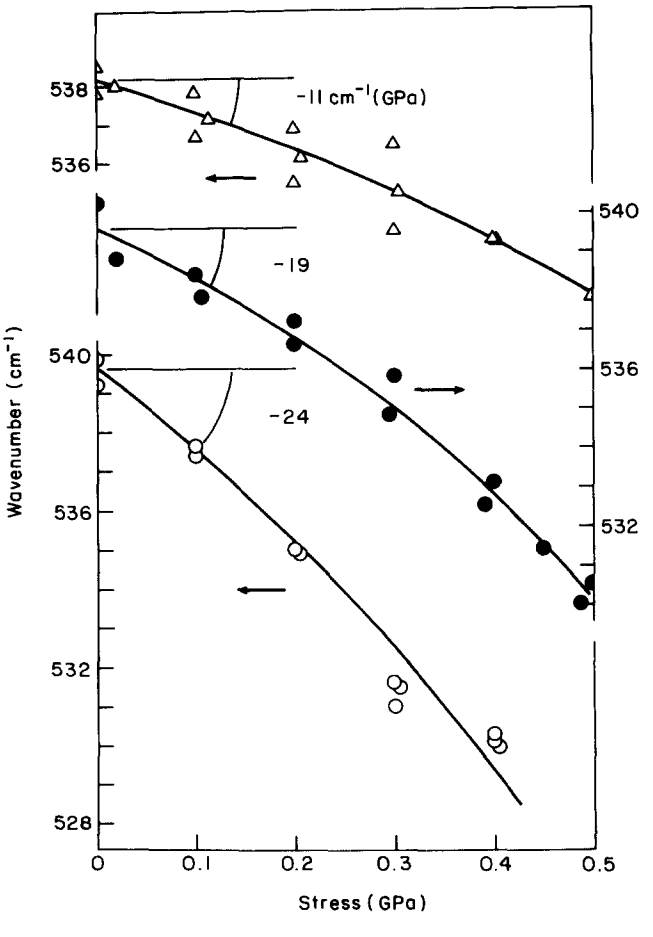

Figure 2 Raman frequency shift induced by tensile stress applied to POM samples with different draw ratios: $\lambda = 34$ (△), 17 (●) and 7.3 (○)

samples with different λ over and above that due to experimental error. This observation is confirmed with good reproducibility. The frequency-shift factor is estimated as follows:

$\lambda = 34$	$\Delta\tilde{\nu}/\Delta\sigma_{bulk} = -11\,cm^{-1}/GPa$
17	-19
7.3	-24

PE. Figure 3 shows the Raman spectra of PE samples measured under tensile stress for the skeletal stretching bands, i.e. ν_s (CC), the symmetric stretching mode at $1131\,cm^{-1}$, and ν_{as} (CC), the antisymmetric stretching mode at $1064\,cm^{-1}$. In *Figure 4* the frequency is plotted against bulk stress for these bands. A tendency for a low-frequency shift is observed, similarly to the case of POM, but the shift factor is very small and no difference among samples is detected. Within experimental error, the frequency shift is estimated as ca. $-6.0\,cm^{-1}/GPa$ for ν_{as} (CC) and $-4.5\,cm^{-1}/GPa$ for ν_s (CC) for all the samples with different draw ratios.

Interpretation of the experimental Raman results by the mechanical series model

The above-mentioned experimental fact that the stress-induced Raman frequency shift is dependent upon the draw ratio of the samples is consistent with the behaviour of the apparent crystallite modulus E_c^{app}, as pointed out in the 'Introduction'. Thus the experimental results of X-ray diffraction and Raman spectroscopic measurements are difficult to interpret reasonably in terms of a homogeneous stress distribution within the sample or the simple mechanical series model, because this model requires independence of the elastic behaviour of the crystalline part upon the sample morphology. So, let us try to analyse the experimental results based on another type of mechanical model.

Interpretation based on the complex mechanical model

It may be possible, of course, to utilize the complicated mechanical models for interpreting the above-mentioned experimental results. But it is better to employ a model that is as simple as possible because the introduction of many undefined parameters will have the danger of resulting in a fruitless arithmetical game. In the present paper we will employ the so-called Takayanagi model (*Figure 5*), which was utilized by Ward *et al.*[2,3] for interpretation of E_c^{app}. In another paper[13], Ward *et al.* proposed the three-component model consisting of the crystalline, amorphous and aligned non-crystalline phases, which might be better in interpreting the mechanical behaviour of POM. But even the simpler mechanical model used here, i.e. the two-component model of crystalline and amorphous phases, can reproduce the essential mechanical behaviour of POM and PE samples quite satisfactorily, as stated below. Although the Takayanagi model has two ways of combining crystalline and amorphous parts (parallel–series and series–parallel models; see *Figure 5*), the two cases do not give very different final results and so the parallel–series model will mainly be used in the present paper. In order to establish the reasonableness of this mechanical model, we will first try to analyse systematically and consistently both E_c^{app} and E_{bulk} data reported so far[9,13–17] and evaluate the parameters a and b

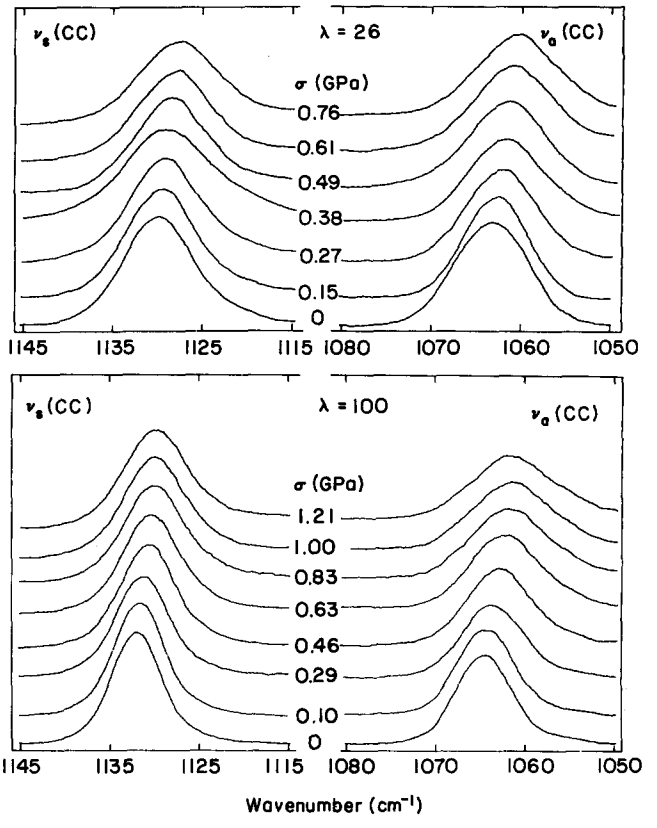

Figure 3 Polarized Raman spectra measured under tensile stress for PE samples with draw ratios of 26 and 100

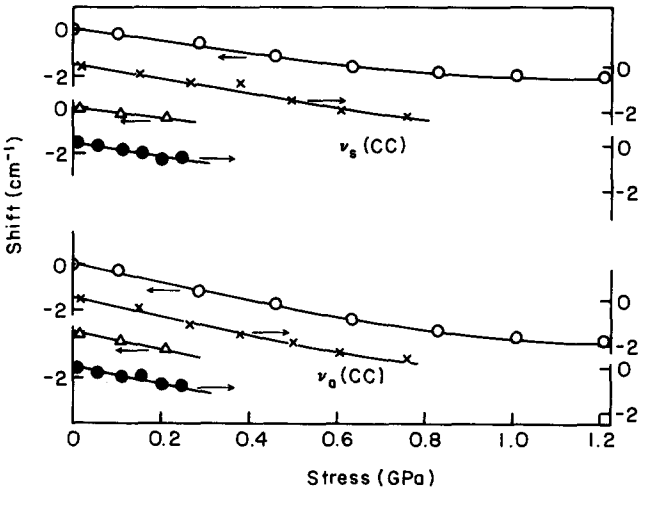

Figure 4 Raman frequency shift induced by tensile stress applied to PE samples with different draw ratios: $\lambda = 100$ (○), 26 (×), 10 (△) and 6.8 (●)

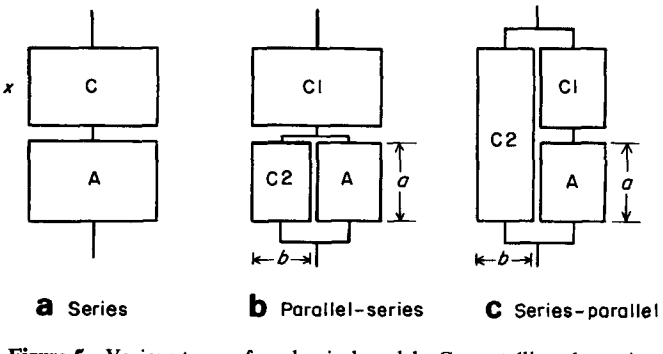

Figure 5 Various types of mechanical models: C, crystalline phase; A, amorphous phase

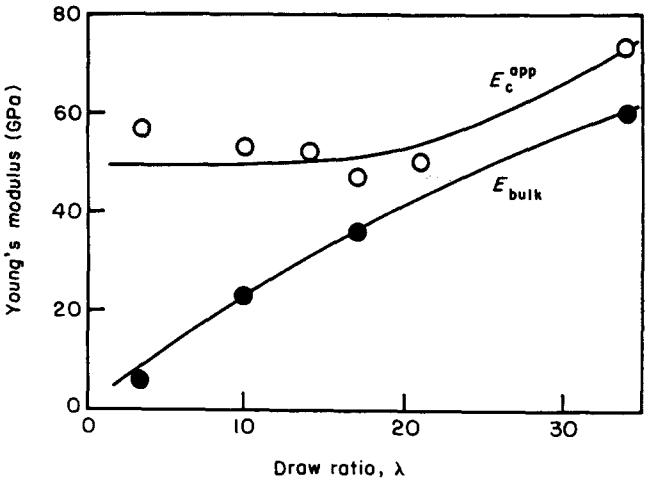

Figure 6 Reported experimental values of E_c^{app} and E_{bulk} of POM samples plotted against draw ratio λ[5,9,13,14,17]

which are necessary for the quantitative interpretation of the Raman data.

Confirmation of the reasonableness of parallel–series model

POM. *Figure 6* shows the dependence of the data of E_c^{app} and E_{bulk} upon the draw ratio λ of the POM samples observed at room temperature[5,9,13,14]. (It should be noted here that all the samples listed in this figure are drawn and annealed under essentially the same conditions: drawn at 140–170°C and annealed at 150–170°C. Therefore we may discuss the mechanical behaviour of these samples on a common basis.) In the low λ range, E_c^{app} is seen to be apparently constant irrespective of λ but E_{bulk} increases greatly with λ. For the sample with high λ, however, E_c^{app} is appreciably higher than that for the low λ samples (more than can be due to experimental error). At the same time, even E_{bulk} exceeds the E_c^{app} values of the low λ samples! So, let us try to interpret the whole data of E_c^{app} and E_{bulk} systematically based on a unique value of the true crystallite modulus E_c^{true}.

In the parallel–series model, the degree of crystallinity x is given by:

$$x = 1 - a + ab \tag{1}$$

where the parameters are defined as shown in *Figure 5b*. The strains of the crystalline components 1 and 2 (ε_1 and ε_2) are different from each other. X-ray diffraction observes their average value[3]:

$$\langle \varepsilon_c \rangle = \frac{1-a}{x}\varepsilon_1 + \frac{ab}{x}\varepsilon_2$$

$$= \frac{1-a}{x}\frac{\sigma_{bulk}}{E_c^{true}} + \frac{ab}{x}\frac{\sigma_{bulk}}{bE_c^{true} + (1-b)E_a} \tag{2}$$

where E_a is Young's modulus of the amorphous component. Then, E_c^{app} and E_{bulk} are written as follows:

$$E_c^{app} = \frac{\sigma_{bulk}}{\langle \varepsilon_c \rangle} = E_c^{true} x \left(1 - a + \frac{ab}{b + (1-b)E_a/E_c^{true}}\right)^{-1} \tag{3}$$

$$E_{bulk} = \frac{\sigma_{bulk}}{\varepsilon_{bulk}} = \left(\frac{1-a}{E_c^{true}} + \frac{a}{bE_c^{true} + (1-b)E_a}\right)^{-1} \tag{4}$$

As seen in these equations (1)–(4), E_c^{app} and E_{bulk} are functions of E_c^{true}, E_a, a and x. Of these, E_c^{true} and E_a are common to all the samples and a and x are dependent on the draw ratio λ. It is desirable to reduce the number of parameters to be determined to as few as possible. Concerning the degree of crystallinity x, Komatsu *et al.*[18] reported a set of experimental data measured by various methods such as n.m.r., d.s.c. and X-ray diffraction. Their results are reproduced in *Figure 7*. The crystallinity estimated using the density is not considered very suitable to adopt here, because the POM samples contain voids, to a greater or lesser degree. The value of x is dependent only on λ but independent of the sample preparation conditions (the pressurized drawing method, the ordinary drawing process, etc.). As seen in *Figure 7*, their data for x, as a function of λ, may be reliable and so are adopted here, because the values estimated by the three different methods are not dispersed very much. In the actual calculation, the average values indicated by asterisks are utilized. As for the amorphous modulus E_a, the final result is not so dependent on the value of E_a over an acceptable range of variation, as stated later. So, in the present calculation the value reported by Ward *et al.*[13] will be employed with a slight modification: $E_a = 3.7$ GPa at room temperature. Using these values of x (as a function of λ) and E_a, we calculated E_c^{app} and E_{bulk} of each sample against the parameter a with a unique constant E_c^{true} common to all the samples. *Figure 8* shows an example for the sample with $\lambda = 14$. In this case, $x = 0.64$ from *Figure 7*. If $E_c^{true} = 109$ GPa is used as a trial value, which is the theoretically calculated value based on the vibrational spectroscopic data without any consideration of thermal motion[9], a suitable solution for a is not found which can reproduce both the observed E_c^{app} and E_{bulk} satisfactorily and consistently within experimental error (about $\pm 10\%$): the calculated E_c^{app} is, on the whole, too high compared with the observed one. This means that the selected E_c^{true} value should be reduced much more. After repeating a trial-and-error process, $E_c^{true} = 75$ GPa is found to satisfy the observed data reasonably, when the a value is about 0.4. In other words, if we choose $E_c^{true} \simeq 75$ GPa, a unique solution for a can exist which satisfies both E_c^{app} and E_{bulk} consistently. Carrying out a similar process for all the

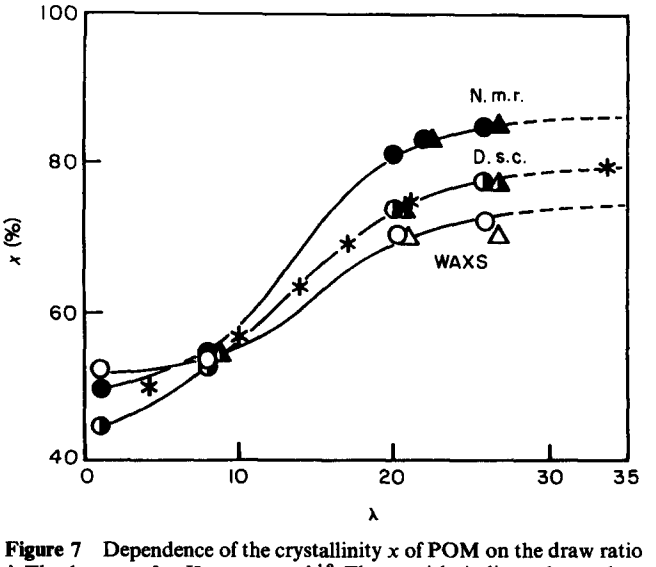

Figure 7 Dependence of the crystallinity x of POM on the draw ratio λ. The data are after Komatsu *et al.*[18]. The asterisks indicate the x values utilized in the calculation of E_c^{app} and E_{bulk} (refer to *Table 1*)

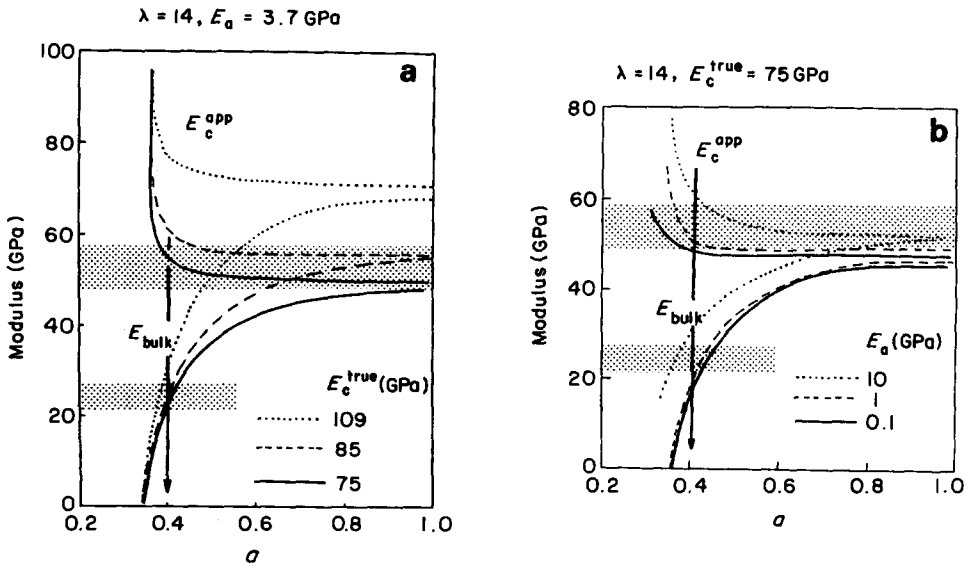

Figure 8 (a) Calculated E_c^{app} and E_{bulk} of POM as a function of the parameter a for various values of E_c^{true}. The observed values with an estimated experimental error of 10% are indicated by the shaded areas. (b) The effect of E_a on the calculated E_c^{app} and E_{bulk}, where E_c^{true} is 75 GPa

samples, we can determine the most suitable values of a and a common value of E_c^{true}. The results are summarized in *Table 1*. In *Figure 8b* is shown the effect of the amorphous modulus E_a on the calculated values of E_c^{app} and E_{bulk}. In this example of *Figure 8b* the unique parameter a is limited to around 0.4 and a too large modulus of E_a, 10 GPa, cannot give a suitable a value which satisfies both E_c^{app} and E_{bulk}. Such a situation is seen for all the samples with different draw ratios. The three-component model proposed by Ward *et al.*[13], which includes the contribution from the aligned non-crystalline component, may require us to utilize an amorphous modulus E_a dependent upon the draw ratio λ; such a consideration might be necessary especially for the sample with high draw ratio ($\lambda = 14$–34). But, as seen in this figure (and also for the case $\lambda = 34$, not indicated here), a slight variation of E_a over a reasonably acceptable range does not affect the final result very much. *Figure 9* shows a comparison between the observed and calculated values of E_c^{app} and E_{bulk} for all the samples, where the straight line represents complete coincidence between the observed and calculated moduli. In the case of $E_c^{true} =$ 109 GPa, E_{bulk} can be fitted but E_c^{app} cannot be explained reasonably; the calculation gives much larger E_c^{app} compared with the observed value. For $E_c^{true} = 75$ GPa, in contrast, both E_c^{app} and E_{bulk} can be explained for all the samples within the allowed experimental error. (In *Figure 10* is shown the case of the series–parallel model (*Figure 5c*) and the result is essentially the same as that of the parallel–series model.) On taking into consideration the experimental error, the actual E_c^{true} may be in the range 68–82 GPa. The difference between the theoretical E_c^{true} (109 GPa) and the estimated E_c^{true} (75 GPa) is considered to originate from the effect of thermal motion of a molecular chain at room temperature: the detailed discussion will be presented in a separate paper[17].

Figure 11 shows the dependence of E_{bulk} on the draw ratio λ, where the observed data are quoted from the paper by Komatsu *et al.*[18]. The calculated E_{bulk} fits the observed curve rather well. It should be noted here that the parameters necessary for calculating E_{bulk} are derived from the data by Ward *et al.*[13], Sakurada *et al.*[14], Nakamae *et al.*[5] and the present authors[17] but the calculated E_{bulk} is in good agreement with the values observed independently by Komatsu *et al.*, indicating that E_{bulk} (and the crystallinity x) is determined almost uniquely by λ, as pointed out by Ward *et al.*[19]. *Figure 12* shows the dependence of the parameters a and b on λ. *Figure 13* illustrates some examples of the mechanical models for samples with different λ. As the draw ratio λ increases, a decreases and b increases gradually. In the case of low λ, the parallel crystalline component 2 is very small in population and therefore the sample might be assumed to satisfy apparently the mechanical series model[1], although the effect of this parallel component on E_c^{app} is never negligible. This is consistent with an approximate constancy of the observed E_c^{app} in this range of λ (see *Figure 6*). As λ increases further, the parallel crystalline component fraction increases and the mechanical series model is not applicable. Although the mechanical model is a mathematical concept and does not necessarily correspond directly to the structural model, such an increment in the parallel crystalline component may suggest an increase in extended tie chains within the sample[19]. In the above calculation the effect of chain orientation is not taken into account. But, as reported[18], the degree of orientation mostly saturates up to 98% even for samples with λ of 7–8. Therefore an orientation effect is neglected here in an approximation. It may also be possible to consider the effect of low chain

Table 1 Comparison of observed and calculated Young's moduli E_c^{app} and E_{bulk} of POM and the parameters x, a and b determined

Draw ratio, λ	E_c^{app} (GPa)		E_{bulk} (GPa)				
	Obs.[a]	Calc.[b]	Obs.[a]	Calc.[b]	x	a	b
4	57	59	6	9	0.50	0.51	0.02
10	53	48	23	21	0.56	0.50	0.12
14	52	55	24	22	0.64	0.40	0.10
17	47	54	36	40	0.69	0.45	0.31
21	50	58	38	43	0.75	0.35	0.29
34	73	61	60	53	0.80	0.36	0.44

[a] Quoted from refs 5, 9, 13, 14 and 17
[b] $E_c^{true} = 75$ GPa, $E_a = 3.7$ GPa

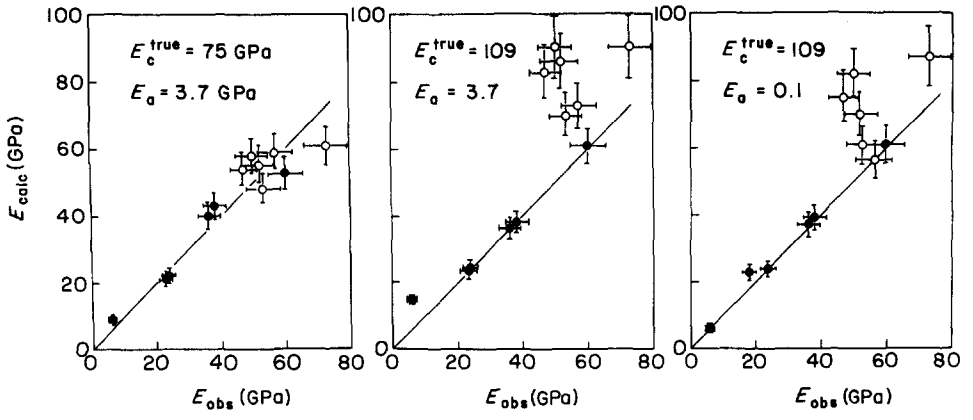

Figure 9 A comparison of the calculated and observed Young's moduli E_c^{app} (○) and E_{bulk} (●) of POM for the various E_c^{true} and E_a based on the parallel–series model. The straight 45° line indicates complete coincidence between the calculated and observed values

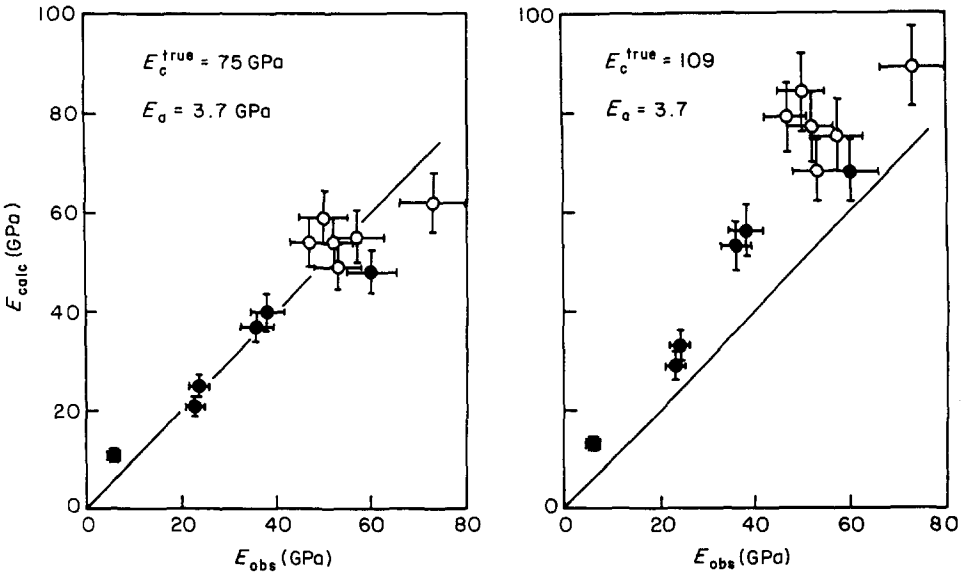

Figure 10 A comparison of the calculated and observed Young's moduli E_c^{app} (○) and E_{bulk} (●) of POM for the various E_c^{true} based on the series-parallel model

orientation, which reduces the crystallite modulus along the draw direction remarkably, as included 'formally' in the soft amorphous component.

PE. A similar treatment was also carried out for PE. *Figure 14* shows the reported λ dependence of E_c^{app} and E_{bulk} for PE samples at room temperature[3,15,16]. In *Figure 15* is shown the relationship between the observed and calculated Young's moduli of PE, indicating the reasonableness of the parameters utilized: $E_c^{true} = 260 \pm 10$ GPa and $E_a = 0.5$ GPa[20-22]. *Table 2* lists the parameters determined. *Figure 16* shows plots of x, a and b determined as a function of λ. *Figure 17* shows some illustrations of the mechanical models of PE with different λ. Different from the case of POM, the contribution of the parallel crystalline component (fraction ab) is very small, e.g. $ab = 0.0001$ for $\lambda = 6$, 0.0004 for $\lambda = 18$ and 0.002 for $\lambda = 100$. In other words, a simple mechanical series model may be apparently a good approximation for interpreting the relationship between the crystallite and bulk moduli of PE, although the observed E_c^{app} is always lower than E_c^{true}.

The E_c^{true} estimated at room temperature, 250–270 GPa, is a little lower than the spectroscopically found values of 290 GPa[23] and 281 GPa[24] and the theoretical value of 316 GPa[25]. This may be due to the effect of large-amplitude thermal motion of planar zigzag chains at room temperature. In fact, E_c^{true} evaluated at -150°C is about 290 GPa[26], very close to the theoretical value.

In this way, by choosing physically reasonable numerical values of the parameters, both E_c^{app} and E_{bulk} can be reproduced systematically enough based on the complex mechanical model. In the following section we will analyse the Raman spectral data based on this mechanical model.

Interpretation of the stress-induced Raman frequency shift based on the complex mechanical model

It will be assumed here that the stress-induced Raman frequency shift is given by a unique function of stress. That is to say, the Raman frequency of the vibrational mode in the crystalline region is assumed to shift linearly with stress in a low-stress region:

$$\tilde{\nu} = \tilde{\nu}_0 - \alpha\sigma \tag{5}$$

where α is the intrinsic frequency shift of the crystalline phase. In the parallel–series model shown in *Figure 5*, the tensile stresses applying to the crystalline phases 1 and 2

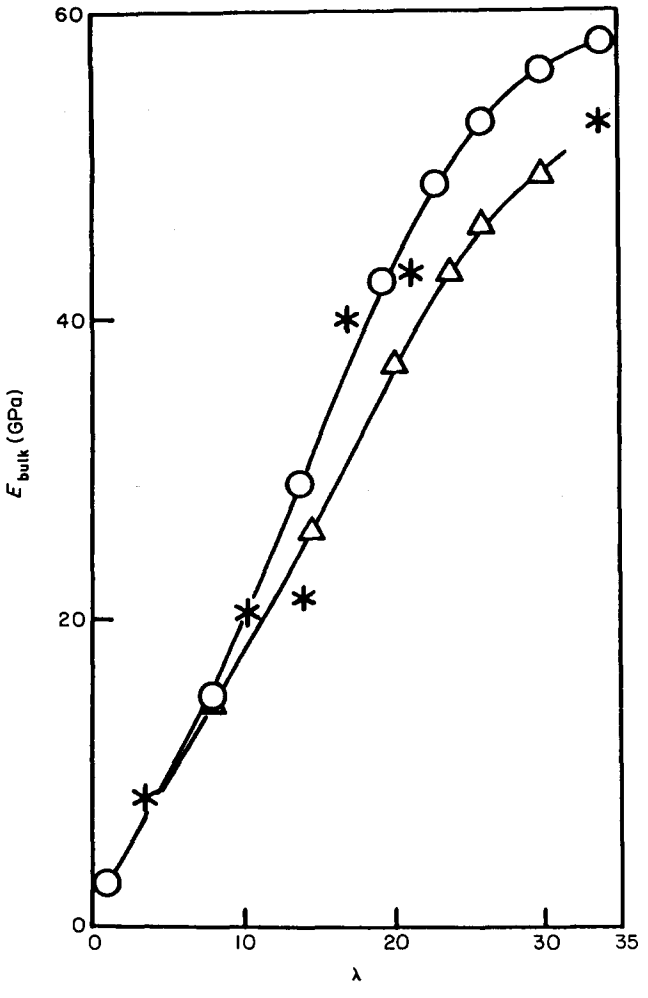

Figure 11 A comparison of the calculated (*) E_{bulk} with the observed data (○ and △) by Komatsu *et al.*[18]: ○, the pressurized drawn samples; △, the ordinarily drawn samples

are expressed in terms of the bulk stress σ_{bulk} as follows:

$$\sigma_1 = \sigma_{bulk} \tag{6}$$

$$\sigma_2 = E_c^{true}\sigma_{bulk}/[bE_c^{true} + (1-b)E_a] \tag{7}$$

Therefore the Raman frequency shifts in the crystalline phases 1 and 2 are given by:

$$\tilde{\nu}_1 = \tilde{\nu}_0 - \alpha\sigma_1 = \tilde{\nu}_0 - \alpha\sigma_{bulk} \tag{8}$$

$$\tilde{\nu}_2 = \tilde{\nu}_0 - \alpha\sigma_2 = \tilde{\nu}_0 - \alpha E_c^{true}\sigma_{bulk}/[bE_c^{true} + (1-b)E_a] \tag{9}$$

The observed Raman intensity $I(\tilde{\nu})$ is assumed to be a summation of the intensity for each vibrating oscillator $i(\tilde{\nu})$ or in proportion to the number of oscillators: if N oscillators exist in the crystalline region, then:

$$I(\tilde{\nu}) = Ni(\tilde{\nu}) \tag{10}$$

In the low-stress region, the observed Raman frequency shift is assumed to be an average between $\tilde{\nu}_1$ and $\tilde{\nu}_2$ weighted with peak intensity. Using equations (8)–(10), the apparent shift $\langle\tilde{\nu}\rangle$ is expressed as follows:

$$\langle\tilde{\nu}\rangle = \frac{I_1(\tilde{\nu})\tilde{\nu}_1 + I_2(\tilde{\nu})\tilde{\nu}_2}{I_1(\tilde{\nu}) + I_2(\tilde{\nu})} \tag{11}$$

$$= \frac{(1-a)\tilde{\nu}_1}{x} + \frac{ab\tilde{\nu}_2}{x}$$

$$= \tilde{\nu}_0 - p\sigma_{bulk} \tag{12}$$

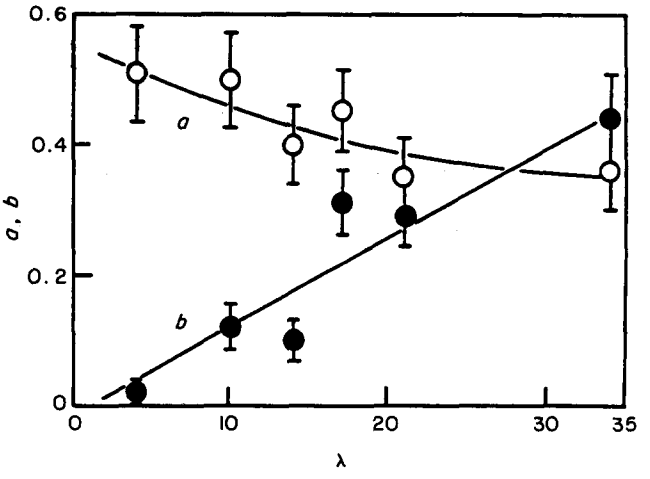

Figure 12 A change in the determined parameters a and b for the draw ratio λ of POM

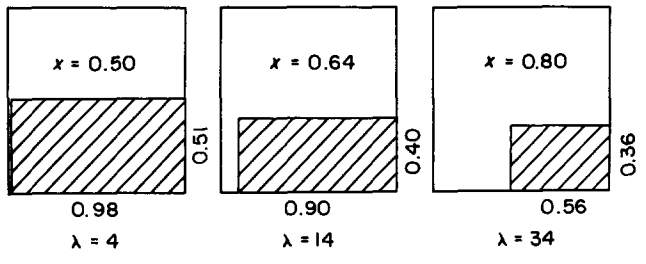

Figure 13 Some illustrations of mechanical models for the POM samples with different draw ratios

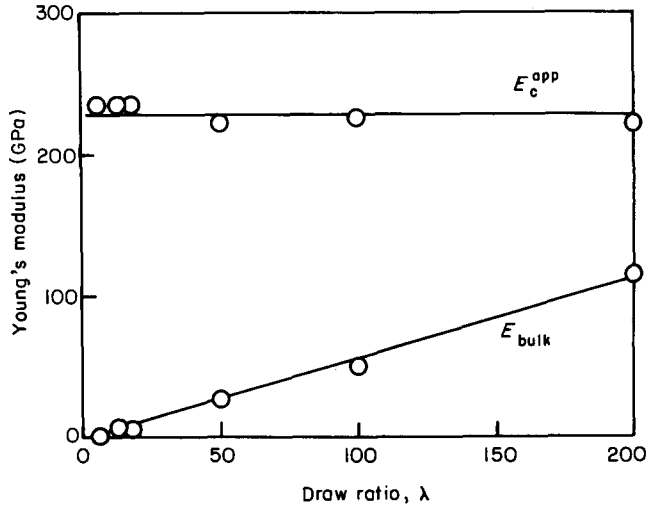

Figure 14 Reported experimental values of E_c^{app} and E_{bulk} of the PE samples with various draw ratios[3,15,16]

Table 2 Comparison of observed and calculated Young's moduli E_c^{app} and E_{bulk} of PE and the parameters x, a and b utilized

Draw ratio, λ	E_c^{app} (GPa)		E_{bulk} (GPa)				
	Obs.[a]	Calc.[b]	Obs.[a]	Calc.[b]	x	a	b
6	235	241	0.64	1.4	0.59	0.41	0.0002
13	235	214	6.9	6.4	0.76	0.24	0.004
18	235	231	4.7	5.0	0.80	0.20	0.002
50	222	238	27	28	0.90	0.10	0.01
100	225	236	50	46	0.90	0.10	0.02
200	222	248	115	116	0.95	0.05	0.04
300	229	250	170	167	0.96	0.04	0.07

[a] Quoted from refs 3, 15 and 16
[b] $E_c^{true} = 260$ GPa, $E_a = 0.5$ GPa

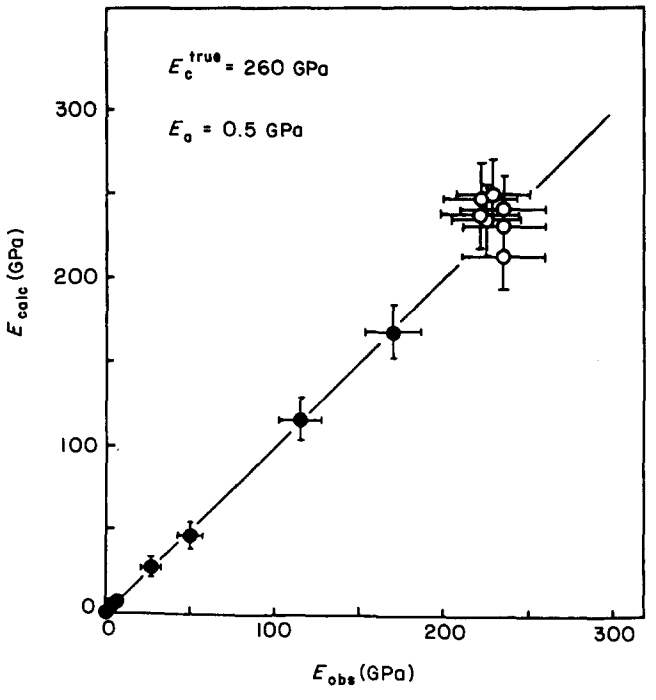

Figure 15 A comparison of the calculated and observed Young's moduli E_c^{app} (○) and E_{bulk} (●) of PE samples. E_c^{true} = 260 GPa and E_a = 0.5 GPa. The straight 45° line indicates complete agreement between the observed and calculated moduli

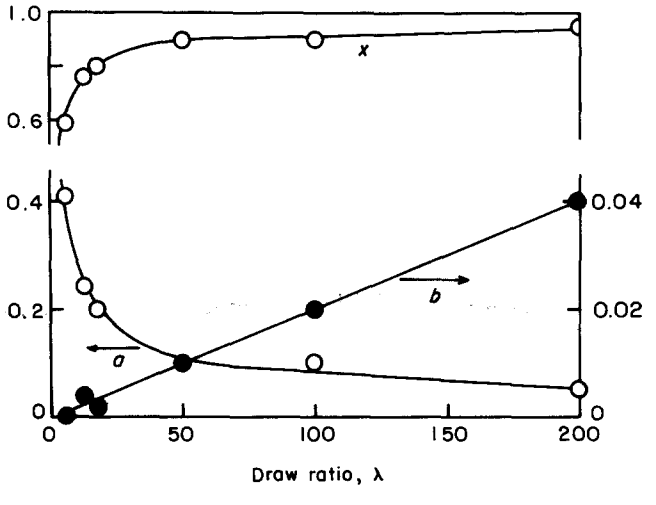

Figure 16 A change in the parameters x, a and b determined for the draw ratio of PE samples

where

$$p=\frac{\alpha}{x}\left(1-a+\frac{abE_c^{true}}{bE_c^{true}+(1-b)E_a}\right)$$
$$=\alpha(E_c^{true}/E_c^{app})$$
$$=\alpha q \qquad (13)$$
$$q=E_c^{true}/E_c^{app} \qquad (14)$$

Equations (12) and (13) imply that the original shift factor is modified to αq due to the inhomogeneous stress distribution within the sample. Since $q \geqslant 1$, the apparent Raman shift factor p is predicted to be larger than α.

POM. In the case of POM, the apparent shift p is estimated from the initial slope of *Figure 2*. Utilizing the calculated and observed values of E_c^{app} and E_c^{true} listed in *Table 1*, q is evaluated from equation (14). A plot of p vs. q should be a straight line passing through the origin. The result is shown in *Figure 18*. The slope of the straight line gives the intrinsic shift factor for the skeletal bending mode as:

$$\alpha \simeq -11\,cm^{-1}/GPa$$

PE. As pointed out in the previous section, the Raman frequency shift induced by the tensile stress is almost independent of the draw ratio of the sample. Such a situation is also seen for E_c^{app}: for all the samples utilized here E_c^{app} is 220–230 GPa. Since the estimated E_c^{true} is about 250–270 GPa, q is calculated to be about 1.2 from equation (14). Using the observed frequency shift data ($p[\nu_{as}(CC)] = -6.0\,cm^{-1}/GPa$ and $p[\nu_s(CC)] = -4.5\,cm^{-1}/GPa$), the intrinsic shift factors are evaluated as follows:

$$\alpha = p/q \simeq -5.0\,cm^{-1}/GPa \quad \text{for } \nu_{as}(CC)$$
$$-3.8\,cm^{-1}/GPa \quad \text{for } \nu_s(CC)$$

As clarified in the case of POM, the apparent frequency shift is larger for the sample with lower draw ratio or the sample with lower fraction of parallel crystalline component. In equation (7), E_c^{true} can be assumed to be much larger than E_a and then σ_2 is approximated as:

$$\sigma_2 = E_c^{true}\sigma_{bulk}/[bE_c^{true}+(1-b)E_a] \simeq \sigma_{bulk}/b \qquad (15)$$

The value of b is small for the low λ sample, and then σ_2 becomes very large. That is to say, the tensile stress acting on the parallel part is concentrated onto the crystalline phase 2, resulting in a larger shift than for component 1.

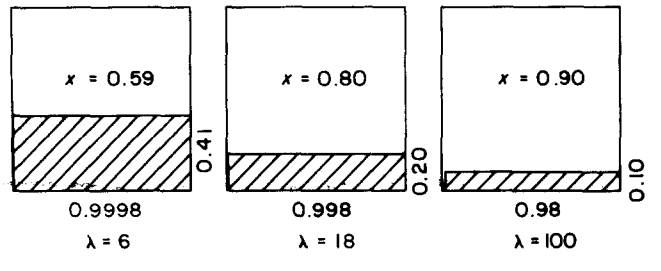

Figure 17 Some illustrations of the mechanical models of PE with different draw ratios

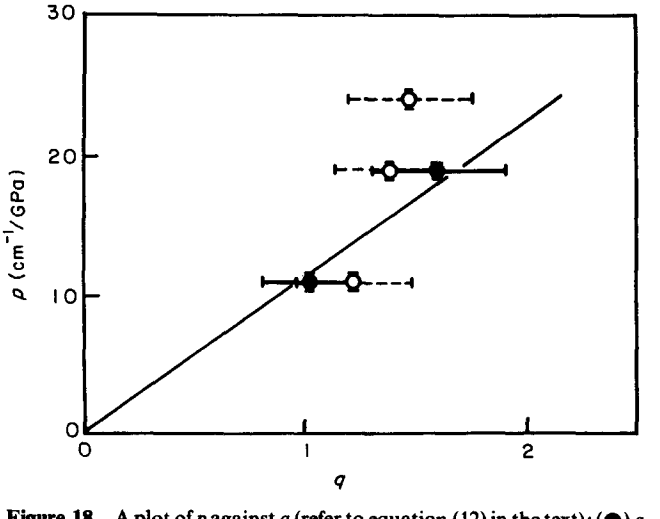

Figure 18 A plot of p against q (refer to equation (12) in the text): (●) q values obtained from the observed E_c^{app} and E_c^{true} ($q = E_c^{true}/E_c^{app}$); (○) q values obtained from the calculated E_c^{app}, where the parameters x, a and b for the sample with $\lambda = 7.3$ are estimated by interpolating the curves of *Figure 12*

Then the apparent peak shift becomes more remarkable for such a low λ sample. (In the case of the crystallite modulus, the strain of the stress-concentrated parallel crystalline part becomes larger than the crystalline part 1, and thus the apparent crystallite modulus is observed to be lower than the intrinsic true modulus.) Actually, of course, we must also take into account the role of the relative populations of each crystalline component in evaluating the apparent frequency shift due to the overlap of these two components. So, in the next section, we will simulate the Raman frequency shift by calculating the change in the spectral profile under the tensile stress.

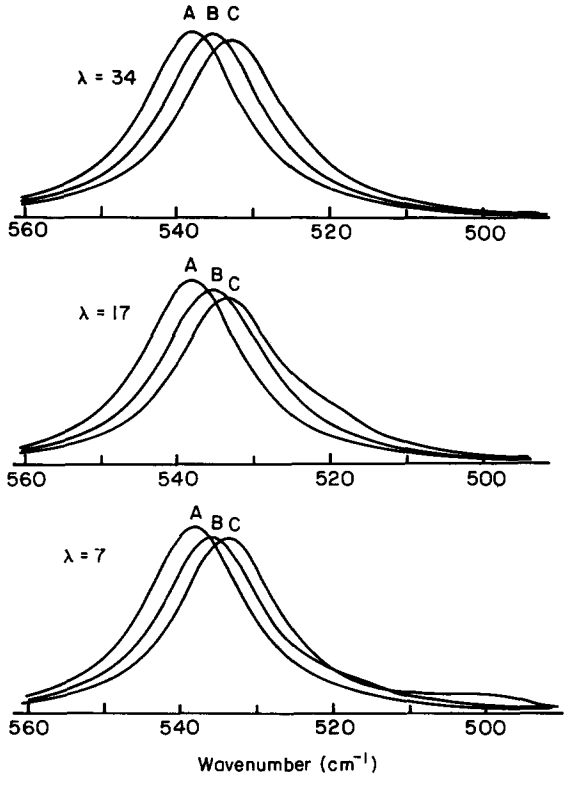

Figure 19 Raman band shift under tensile stresses calculated for POM samples with various draw ratios (the utilized parameters are referred to in *Table 1*): A, 0 GPa; B, 0.2 GPa; C, 0.4 GPa

A simulation of vibrational shift under tensile stress

The band profile of a vibrating oscillator $g(\tilde{\nu})$ is assumed to be expressed by the following Lorentzian function:

$$g(\tilde{\nu})=\frac{g_0}{(\tilde{\nu}-\tilde{\nu}_0)^2+r^2} \tag{16}$$

where $\tilde{\nu}_0$ is the peak frequency, g_0/r^2 is the peak height and $2r$ is the halfwidth. By introducing an equation for the stress dependence of frequency (equation (5)) instead of $\tilde{\nu}_0$ in equation (16):

$$g(\tilde{\nu};\sigma)=\frac{g_0}{(\tilde{\nu}-\tilde{\nu}_0+\alpha\sigma)^2+r^2} \tag{17}$$

where g_0 and r are assumed to be independent of stress. The whole profile for the crystalline parts is given by:

$$G(\tilde{\nu})\propto\frac{1-a}{x}g(\tilde{\nu};\sigma_1)+\frac{ab}{x}g(\tilde{\nu};\sigma_2) \tag{18}$$

Substituting equations (6) and (7) into equations (17) and (18), we obtain:

$$G(\tilde{\nu})\propto\frac{1-a}{x}\frac{g_0}{(\tilde{\nu}-\tilde{\nu}_0+\alpha\sigma_{\text{bulk}})^2+r^2}+\frac{ab}{x}\frac{g_0}{\{\tilde{\nu}-\tilde{\nu}_0+\alpha\sigma_{\text{bulk}}E_c^{\text{true}}/[bE_c^{\text{true}}+(1-b)E_a]\}^2+r^2} \tag{19}$$

Using the numerical values of the parameters, $G(\tilde{\nu})$ is calculated for a given tensile stress; r is assumed to be $8\,\text{cm}^{-1}$ for POM and $4\,\text{cm}^{-1}$ for PE.

POM. The calculated results are shown in *Figure 19*. In *Figure 20* are shown the contributions of the two crystalline components to the band profile. As pointed out in equation (15), the band position of the crystalline component 2 shifts more than that of component 1 because of stress concentration. Such a tendency is more remarkable for the sample with lower draw ratio λ. Then the resultant apparent peak position is observed to shift much more for such a sample. At the same time the band

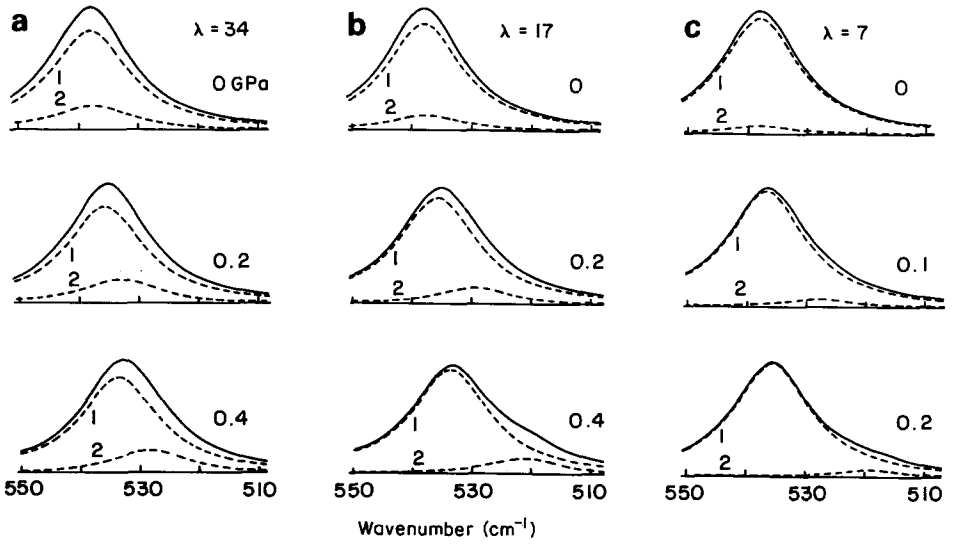

Figure 20 Effect of tensile stress on the Raman band profiles and the contribution of the crystalline components 1 and 2 calculated for POM samples with different draw ratios

profile becomes asymmetric and broader; in an extreme case a shoulder begins to be observed for high stress. In the actual sample, the stress distribution may be more complicated than the present simple mechanical model and more components may be needed in the calculation. Then the band profile will become more continuous and broader with increasing stress[27,28]. Such a prediction corresponds well to the broadening actually observed in the band profile shown in *Figure 1*. In *Figure 18* the apparent frequency shift of a peak position is estimated as follows:

$$\text{for } \lambda = 34, \quad p \simeq -13\,\text{cm}^{-1}/\text{GPa}$$
$$\text{for } \lambda = 17, \quad p \simeq -18\,\text{cm}^{-1}/\text{GPa}$$
$$\text{for } \lambda = 7, \quad p \simeq -21\,\text{cm}^{-1}/\text{GPa}$$

These values are in good agreement with the observed ones.

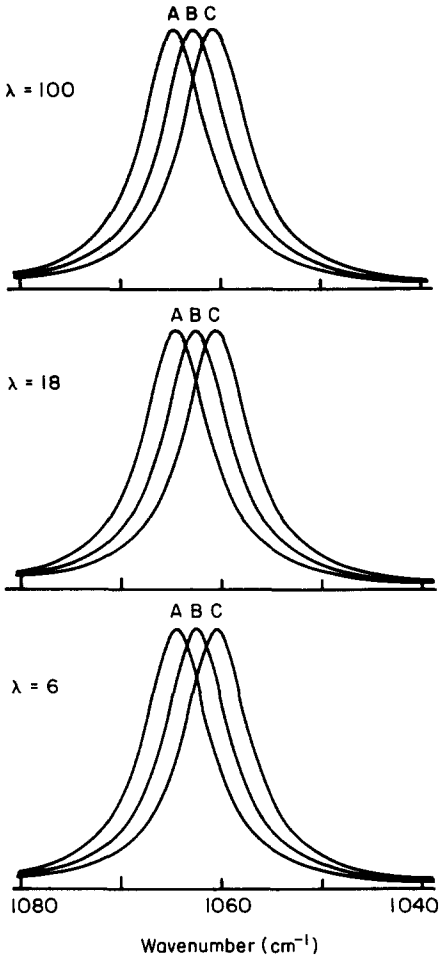

Figure 21 Raman band shift under tensile stresses calculated for PE samples with various draw ratios (the utilized parameters are referred to in *Table 2*): A, 0 GPa; B, 0.5 GPa; C, 1.0 GPa

PE. *Figures 21* and *22* show the dependence of the Raman band profile for various values of the tensile stress. In this case the stress-induced low-frequency shift is almost constant irrespective of the sample. This is because, as pointed out in the previous section, the fractional contribution of the second crystalline component is very small (see *Figure 17*). A small shift factor may also make it difficult to detect a slight difference in the Raman shift among the samples. The bandwidth may become, in principle, broader with increasing stress but the change is very small. In fact the band broadening of PE is not so remarkable compared with the case of POM.

CONCLUSIONS

In the present paper we have discussed the mechanical model for crystalline POM and PE. In the interpretation of the Young's modulus and stress-induced Raman frequency shift, at least, the so-called parallel–series model (or almost equivalently the series–parallel model) is found to be more appropriate than the simple mechanical series model. As pointed out, however, the series model may apparently be a good approximation for samples with not very high draw ratio, because the contribution of the parallel crystalline component is small.

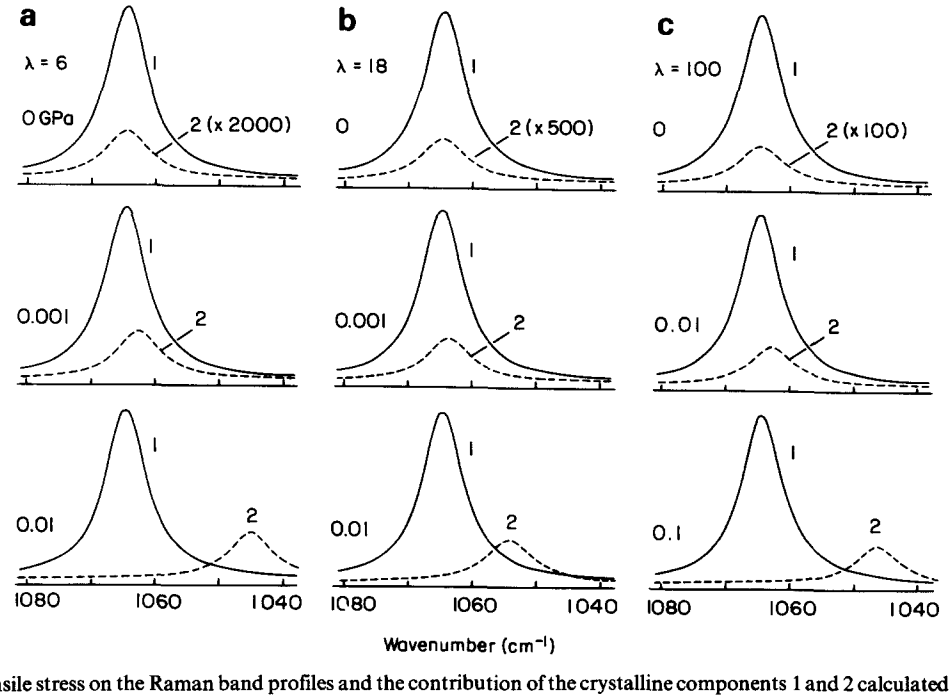

Figure 22 Effect of tensile stress on the Raman band profiles and the contribution of the crystalline components 1 and 2 calculated for PE samples with different draw ratios

In fact the reported E_c^{app} is not very dispersed for samples with low λ, although the value itself is a little lower than E_c^{true}. But, for samples prepared with ultra-high draw ratio, the contribution of the parallel component cannot be neglected and the series model cannot be accepted to interpret the mechanical behaviour of the samples. The discussion developed in this paper should be applied also to the interpretation of the temperature dependence of the crystallite modulus. The details will be reported in a separate paper[17].

ACKNOWLEDGEMENTS

The authors are grateful to Emeritus Professor Hiroyuki Tadokoro for his continuing encouragement. This work was supported in part by a Grant-in-Aid for Scientific Research on Priority Areas, New Functionality Materials—Design, Preparation and Control, The Ministry of Education, Science and Culture, Japan.

REFERENCES

1 Sakurada, I. and Kaji, K. *J. Polym. Sci.* (*C*) 1970, **31**, 57
2 Brew, B., Clements, J., Davies, G. R., Jakeways, R. and Ward, I. M. *J. Polym. Sci., Polym. Phys. Edn.* 1979, **17**, 351
3 Clements, J., Jakeways, R. and Ward, I. M. *Polymer* 1978, **19**, 639
4 Nakamae, K., Nishino, T., Okubo, H. and Matsumoto, T. *Polym. Prepr. Jpn.* 1987, **36**, 2441
5 Nakamae, K., Nishino, T., Shimizu, T., Hata, K. and Matsumoto, T. *Polym. Prepr. Jpn.* 1987, **36**, 2438
6 Wu, G., Tashiro, K. and Kobayashi, M. *Rep. Prog. Polym. Phys. Jpn.* 1986, **29**, 297
7 Wu, G., Tashiro, K. and Kobayashi, M. *Macromolecules* to be published
8 Wu, G., Tashiro, K. and Kobayashi, M. *Rep. Prog. Polym. Phys. Jpn.* 1987, **30**, 127
9 Wu, G., Tashiro, K. and Kobayashi, M. *Rep. Prog. Polym. Phys. Jpn.* 1987, **30**, 143
10 Tashiro, K., Kobayashi, M. and Tadokoro, H. *Macromolecules* 1977, **10**, 413; 1978, **11**, 908
11 Komatsu, T., Enoki, S. and Aoshima, A. *Polym. Prepr. Jpn.* 1986, **35**, 3712
12 Nakagawa, K., Konaka, T. and Yamakawa, S. *Polymer* 1985, **26**, 84
13 Jungnitz, S., Jakeways, R. and Ward, I. M. *Polymer* 1986, **27**, 1651
14 Sakurada, I., Ito, T. and Nakamae, K. *J. Polym. Sci.* (*C*) 1966, **15**, 75
15 Nakamae, K. Doctoral Thesis, Kyoto University, 1966
16 Matsuo, M. and Sawatari, C. *Macromolecules* 1986, **19**, 2036
17 Wu, G., Tashiro, K., Kobayashi, M., Komatsu, T. and Nakagawa, K. *Macromolecules* to be published
18 Enoki, S., Komatsu, T. and Aoshima, A. *Polym. Prepr. Jpn.* 1986, **35**, 3716
19 'Ultra-High Modulus Polymers' (Eds. A. Ciferri and I. M. Ward), Applied Science, London, 1979
20 Reding, F. D. *J. Polym. Sci.* 1958, **32**, 487
21 Flocke, H. A. *Kolloid Z.* 1962, **180**, 118
22 Schrveiger, W. H. *Kunststoffe* 1961, **51**, 256
23 Strobl, G. R. and Eckel, R. *J. Polym. Sci., Polym. Phys. Edn.* 1976, **14**, 913
24 Kobayashi, M., Sakagami, K. Tadokoro, H. *J. Chem. Phys.* 1983, **78**, 6391
25 Tashiro, K., Kobayashi, M. and Tadokoro, H. *Macromolecules* 1978, **11**, 914
26 Barham, P. J. and Keller, A. *J. Polym. Sci., Polym. Lett. Edn.* 1979, **17**, 591
27 Zhurkov, S. N., Vettegren, V. I., Korsukov, V. E. and Novak, I. I. *Fracture* 1975, **11**, 789
28 Wool, R. P. *Polym. Eng. Sci.* 1980, **20**, 805